Communication

Deformation Microstructure and Deformation-Induced Martensite in Austenitic Fe-Cr-Ni Alloys Depending on Stacking Fault Energy

YE TIAN, OLEG I. GORBATOV, ANNIKA BORGENSTAM, ANDREI V. RUBAN, and PETER HEDSTRÖM

The deformation microstructure of austenitic Fe-18Cr-(10-12)Ni (wt pct) alloys with low stacking fault energies, estimated by first-principles calculations, was investigated after cold rolling. The ε-martensite was found to play a key role in the nucleation of α′-martensite, and at low SFE, ε formation is frequent and facilitates nucleation of α′ at individual shear bands, whereas shear band intersections become the dominant nucleation sites for α′ when SFE increases and mechanical twinning becomes frequent.

Metastable austenitic stainless steels are of high technical interest due to their pronounced work hardening behavior, providing an attractive ductility in combination with their inherently high corrosion resistance. Part of the high work hardening is due to the deformation-induced martensitic transformation (DIMT), which has been the subject of extensive research in commercial steels.[1–4] Experimental research considering the microstructure of carefully tailored model alloys that can more directly be compared with theoretical predictions of stacking fault energy (SFE) using, for instance, first-principles calculations[5] and

YE TIAN, Ph.D. Candidate, ANNIKA BORGENSTAM, Professor, and PETER HEDSTRÖM, Assistant Professor, are with the Department of Materials Science and Engineering, KTH Royal Institute of Technology, 10044 Stockholm, Sweden. Contact e-mail: yti@kth.se OLEG I. GORBATOV, Postdoctoral Fellow, is with the Department of Materials Science and Engineering, KTH Royal Institute of Technology, and also with the Nosov Magnitogorsk State Technical University, 455000 Magnitogorsk, Russia. ANDREI V. RUBAN, Professor, is with the Department of Materials Science and Engineering, KTH Royal Institute of Technology, and also with the Materials Center Leoben, 8700 Leoben, Austria.

thermodynamics-based modeling[6] is, however, more scarce in the literature. The body-centered cubic (bcc) martensite (α′-martensite, hereinafter referred to as α′) has been claimed to contribute most to the mechanical properties of these alloys, but also the hexagonal close-packed (hcp) martensite (ε-martensite, hereinafter referred to as ε) is important since it is known to contribute to the nucleation of the α′ as well as the mechanical properties. Consensus has not been reached about this to date. Two transformation sequences of the α′ have been reported: (i) γ (austenite, face-centered cubic(fcc)) → ε → α′ and (ii) γ → α′,[3,7–9] and it is today generally accepted that ε can be a transient phase,[10,11] but it is not a necessary precursor for α′.[12,13] Furthermore, it is likely that the transformation sequence differs with the variation of chemical composition, temperature, and strain rate,[14] and that it can be related to SFE and the austenite stability.[15] Clearly, the discussion about the existence of a transient phase relates to the nucleation and growth of α′. In the most commonly applied model of DIMT,[7] intersections of shear bands (SBs, consisting of bundles of intermixed faults, twins, and ε[16,17]) are assumed to be the preferred nucleation sites for α′,[18] but it has also been shown that nucleation at individual SBs,[19–23] grain boundaries,[24] and SB–grain boundary intersections[3] may occur. Another interesting aspect of nucleation of deformation-induced martensite is the suggested difference between stress-assisted and strain-induced nucleation.[7] Perdahcioglu et al.[25,26] have suggested that the main effect of the deformation is the additional mechanical driving force and that the strain, possibly generating potent nucleation sites, is not very important for DIMT. This hypothesis was supported by the modeling in Das et al.[27] who showed that a majority of the literature data relating plastic strain and α′ could be described by considering the stress effect, including strain hardening, alone.

The brief survey presented here shows that further investigations are needed to improve our current understanding of deformation of austenitic stainless steels and in particular the deformation-induced nucleation of martensite. Thus, in the present work we utilize a combination of electron channeling contrast imaging (ECCI) and electron backscatter diffraction (EBSD)[19,28–31] to develop a more quantitative view of deformation-induced nucleation of martensite in austenite with different stabilities and SFEs. The deformation behavior was investigated in ternary Fe-Cr-Ni model alloys with varying nickel contents to incrementally control the austenite stability.

The alloys were produced using arc-melting of pure iron (>99.99 wt pct purity), chromium (>99.99 wt pct purity), and nickel (>99.98 wt pct purity). The chemical compositions of the alloys, their lattice parameters, and calculated SFEs are given in Table I. All alloys were melted four times followed by compressive deformation and homogenization at 1423 K (1150 °C) for 12 hours in

Ar atmosphere. The final disk-shaped samples were obtained by cold rolling. The samples were then austenitized at 1323 K (1050 °C) for 5 minutes followed by quenching in brine. Finally, the samples were cold rolled to 10, 20, and 30pct reduction and characterized using EBSD and ECCI in a JEOL 7800F field emission scanning electron microscope (FESEM). More details about the experimental procedures can be found in our previous work.[32]

The SFEs were evaluated using the axial next-nearest-neighbor Ising model[33]: $\gamma(T) = F^{hcp}(T) + 2F^{dhcp}(T) - 3F^{fcc}(T)$, where $F^{hcp}(T)$, $F^{dhcp}(T)$, and $F^{fcc}(T)$ are the free energies of the ideal hcp, double hcp (dhcp), and fcc structures, respectively. The volumes per atom of the ideal hcp and double hcp (dhcp) structures are the same as for the fcc structure, implying that only the fcc volume needs to be known. The latter was taken from the experimental data for the particular alloys investigated in this work (see Table I). The self-consistent density functional theory total energy calculations were done by the exact muffin-tin orbital (EMTO) method combined with the coherent potential approximation (CPA) to treat the electronic structure of random atomic configurations.[34,35] The finite temperature magnetic state for all elements was treated with the account for longitudinal spin fluctuations in the disordered local moment state.[36] The electronic single-particle excitations were described *via* the Fermi function. The alloys' free energies have been determined as described in Reference 37. The total energies were calculated in the generalized gradient approximation.[38] All the self-consistent EMTO-CPA calculations were performed for the orbital momentum cut-off of $l^{max} = 3$ for the partial waves. The integration over the Brillouin zone was done using $31 \times 31 \times 31$, $31 \times 31 \times 19$, and $31 \times 31 \times 9$ grid of k-points determined according to the Monkhorst–Pack scheme for fcc, hcp, and dhcp, respectively.[39]

The accuracy of the CPA has been checked in the corresponding locally self-consistent Green's function (LSGF) calculations.[40,41] The EMTO-LSGF method has also been used to determine the parameters (on-site screening constants α_{scr} and β_{scr}), describing the contributions of screened Coulomb interactions to the one-electron potential of an alloy component and to the total energy within the single-site formalism.[42,43] The calculated on-site screening constant α_{scr} varies with the structure but slightly with alloy composition, lattice parameter, and temperature. For the fcc structure, α_{scr} is equal to 0.725, 0.777, and 0.824 for Fe, Cr, and Ni, respectively, while β_{scr} is about 1.14.

The calculated SFEs for the investigated alloys are presented in Table I. It can be seen that the 18-10 alloy has a predicted SFE of 6.6 mJ m^{-2} and that the SFE increases with increasing Ni to 12.4 mJ m^{-2} for alloy 18-12. The increasing SFE with increasing Ni is in agreement with previous works in the literature and the values of SFE are also in reasonable agreement with the literature (see, *e.g.*, Reference 44). However, it should be noted that accurate measurements and calculations of SFE for complex alloys are a significant challenge. There are no direct ways of measuring the SFE and the reported range of experimental SFEs is large.[45] Furthermore, exact SFE calculations from first-principles are challenging. For example, the accurate calculation of the finite temperature lattice parameters for austenitic steels is not trivial due to difficult considerations of their finite temperature state.[46] In the present work, the measured lattice parameters for each alloy were used and this is deemed more appropriate for the estimation of SFE of real alloys. On the other hand, the effect of N and C was not included in the calculations and has not been included in other works either. The C and N contents of the experimental alloys are low, but it could still cause an underestimation of the SFEs since small additions of N are most likely increasing the SFE, whereas the effect of C should be quite small.[45] It should also be mentioned that by using the measured lattice parameters in the calculations, the effect of C and N is indirectly accounted for in the present calculations by the changing lattice parameters, since at least at small concentrations of C and N, one can expect that the main effect of these interstitials on the SFE is due to the increase of the lattice parameter.

Figure 1 illustrates the deformation structure of alloy 18-10 after 10 pct reduction. Even at a low degree of deformation, small units of α' are found inside individual SBs and at their intersections. Moreover, α' is also found to grow into the austenite matrix, but the growth is restricted by several adjacent SBs and thus a blocky-type martensite (hereinafter referred to as blocky α') (Figure 1(c)), similar to the structure observed by Weidner[28] and Lecroisey,[18] is seen. These observations illustrate that the austenite stability in alloy 18-10 is so low (illustrated in our previous work[32]) that the local stress produced by the small units of α' within SBs supposedly triggers martensitic transformation nearby and even an autocatalytic process between adjacent sets of SBs yielding the blocky α' (Figure 1(c)).[18,47] Inside individual SBs, most of the structure apart from α' is ε (indicated in Figure 1(a) and (b)). It could be explained that, with rather low SFE, stacking faults (SFs) tend to overlap on every second {111} plane, thus reducing the total energy of these bundles of SFs for forming ε phase. The nucleation sites for α' in alloy 18-10 are mainly

Table I. Chemical Compositions (Wt Pct), Lattice Parameters *a* (Å), and SFEs (mJ m^{-2}) of the Investigated Fe-Cr-Ni Alloys

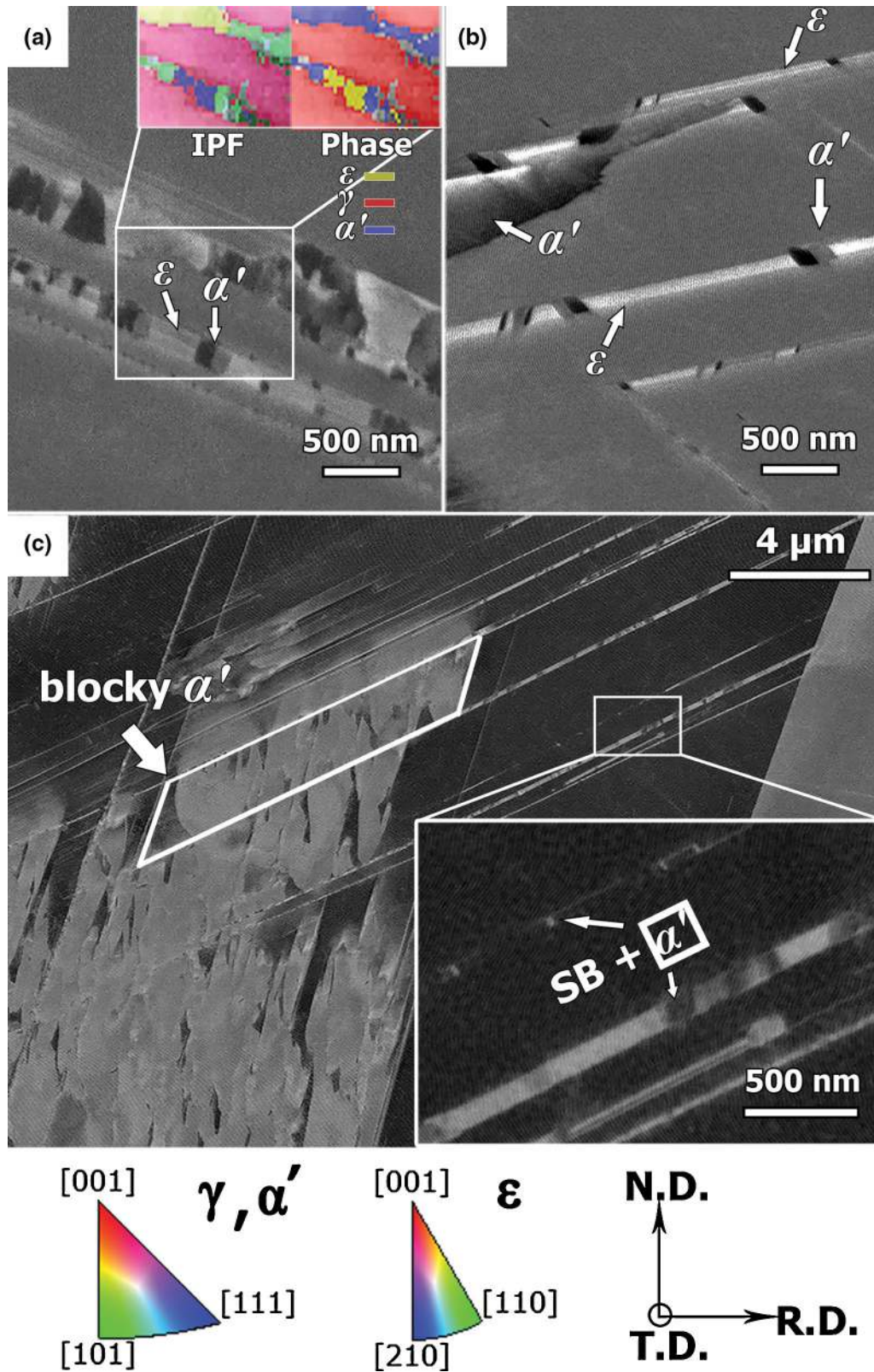| Designation	Fe	Cr	Ni	C	N	W	Ti	a	SFE
18-10	bal.	18.1	9.9	0.002	0.025	—	—	3.5872	6.6
18-10.5	bal.	17.9	10.4	0.004	0.033	0.02	0.09	3.5864	7.8
18-11	bal.	18.1	11.0	0.008	0.046	0.03	—	3.5869	9.6
18-11.5	bal.	18.0	11.5	0.006	0.053	—	—	3.5853	9.8
18-12	bal.	18.1	12.0	0.008	0.055	—	0.03	3.5860	12.4

Fig. 1—Deformation structure at 10pct cold rolling reduction for alloy 18-10: (*a*) correspondence between ECCI and EBSD. The blocky α' martensite is indicated and the inverse pole figure (IPF//R.D.) coloring shows the crystallographic orientations; (*b*) detailed account of the phases in ECCI image; and (*c*) ECCI overview.
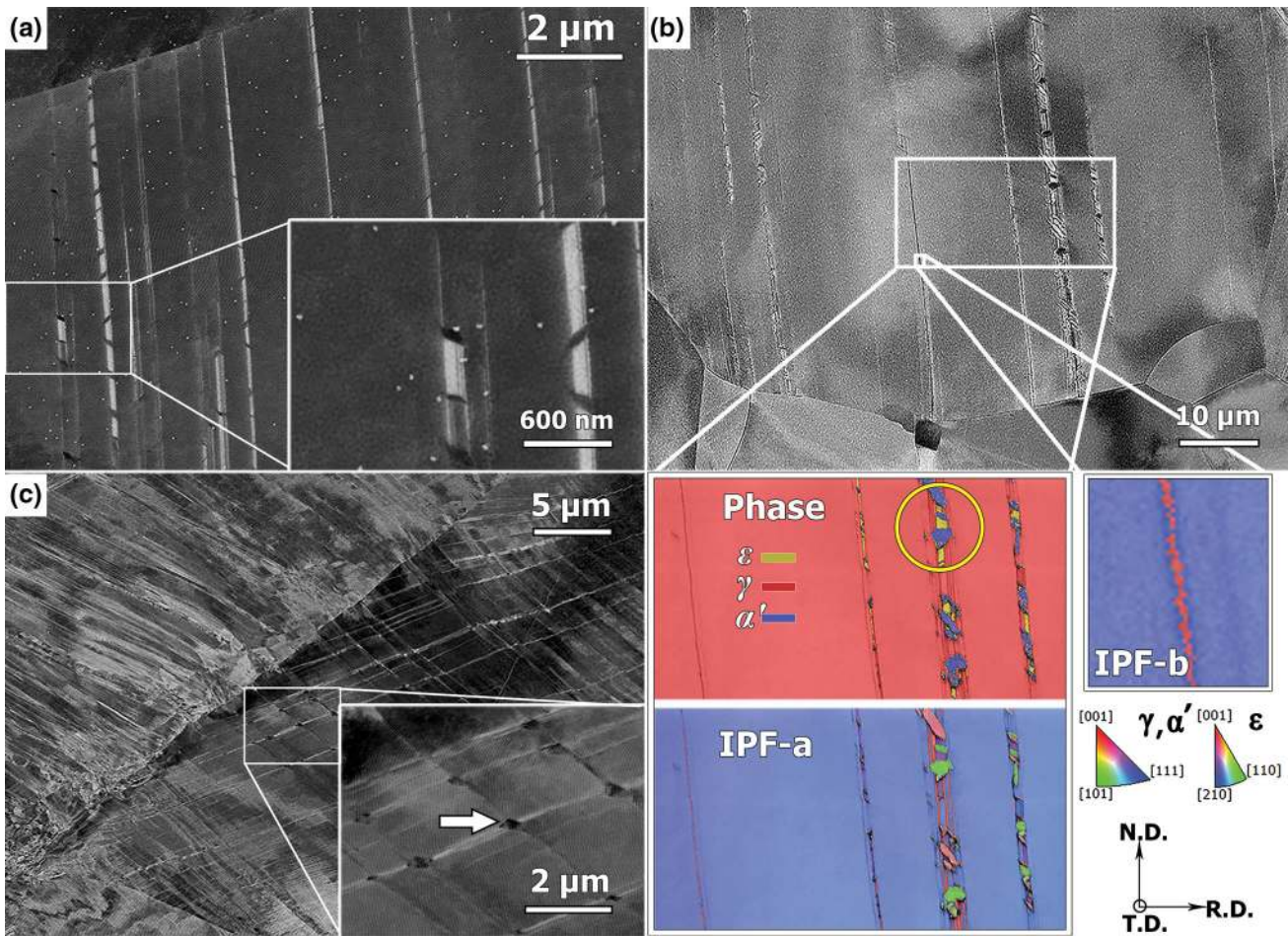
Fig. 2—Deformation structure at 10pct cold rolling reduction for (*a*) alloy 18-10.5, (*b*) alloy 18-11 (IPF-b: mechanical twinning), and (*c*) at 30pct cold rolling reduction for alloy 18-11.5.

individual SBs (inset of Figure 1(c)), similar to the observations on a 301 commercial steel,[23] where the presence of ε has been reported to reduce the activation energy for α' nucleation.[29]

Figure 2(a) shows the deformation structure of alloy 18-10.5 after 10 pct reduction. Similar to alloy 18-10, though there are no clear intersections of SBs in this grain at the early stage of deformation, the formation of α' within individual SBs could be observed. However, there is little blocky α' observed growing into the austenite region as in alloy 18-10 due to the increase of SFE through the addition of Ni.[29]

When further increasing the Ni content to 11 wt pct, another type of SBs appears in the microstructure (Figure 2(b)). Apart from the SBs consisting of small units of α' that were observed in the previous two alloys, SBs consisting of mechanical twins (see additional inverse pole figure (IPF-a//R.D. and IPF-b//R.D.) in Figure 2(b)) are now more prominent in the deformation structure. As SFE rises, the transformation mechanism begins to change from $\gamma \rightarrow \varepsilon \rightarrow \alpha'$ to $\gamma \rightarrow \gamma^{twin} \rightarrow \alpha'$, since mechanical twins become thermodynamically more favorable with increasing Ni addition.[29,48,49] Although it has been reported that mechanical twins could be the nucleation sites for α',[20] it should be noted that individual twins without the help of ε cannot be the preferential area for α' nucleation as

observed (see phase map in Figure 2(b)). However, individual SBs consisting of ε, twins, and SFs can be the nucleation sites for α' at the area where ε forms (indicated by yellow circle in Figure 2). For alloy 18-11.5 with 10pct reduction, the deformation structure appears quite similar to the one of alloy 18-11 but with less SBs.

The deformation structure of alloy 18-11.5 with 30pct reduction is shown in Figure 2(c). Here all α' (see inset of Figure 2(c)) nucleates at intersections of SBs in agreement with the commonly accepted nucleation theory.[7,18] Combined with the observations of nucleation sites for DIMT in alloys 18-10, 18-10.5, and 18-11, it implies that intersections of SBs are more favorable than individual SBs since the "doubly faulted" intersected volumes are almost true bcc structures.[7,50] However, with rather low austenite stability and the existence of ε, it is not necessary to form at the intersections, and since the available nucleation sites for α' within individual SBs are much greater that those at the intersections, nucleation at parallel bands is dominant for alloys with low SFE, *e.g.*, alloy 18-10 in this work or 301 steel in Naraghi *et al.*[23] Similar phenomena have also been observed by Martin *et al.*[19,29,51,52]; however, the mechanism was not explained. A simple explanation of this phenomenon would be the much lower activation energy for α'
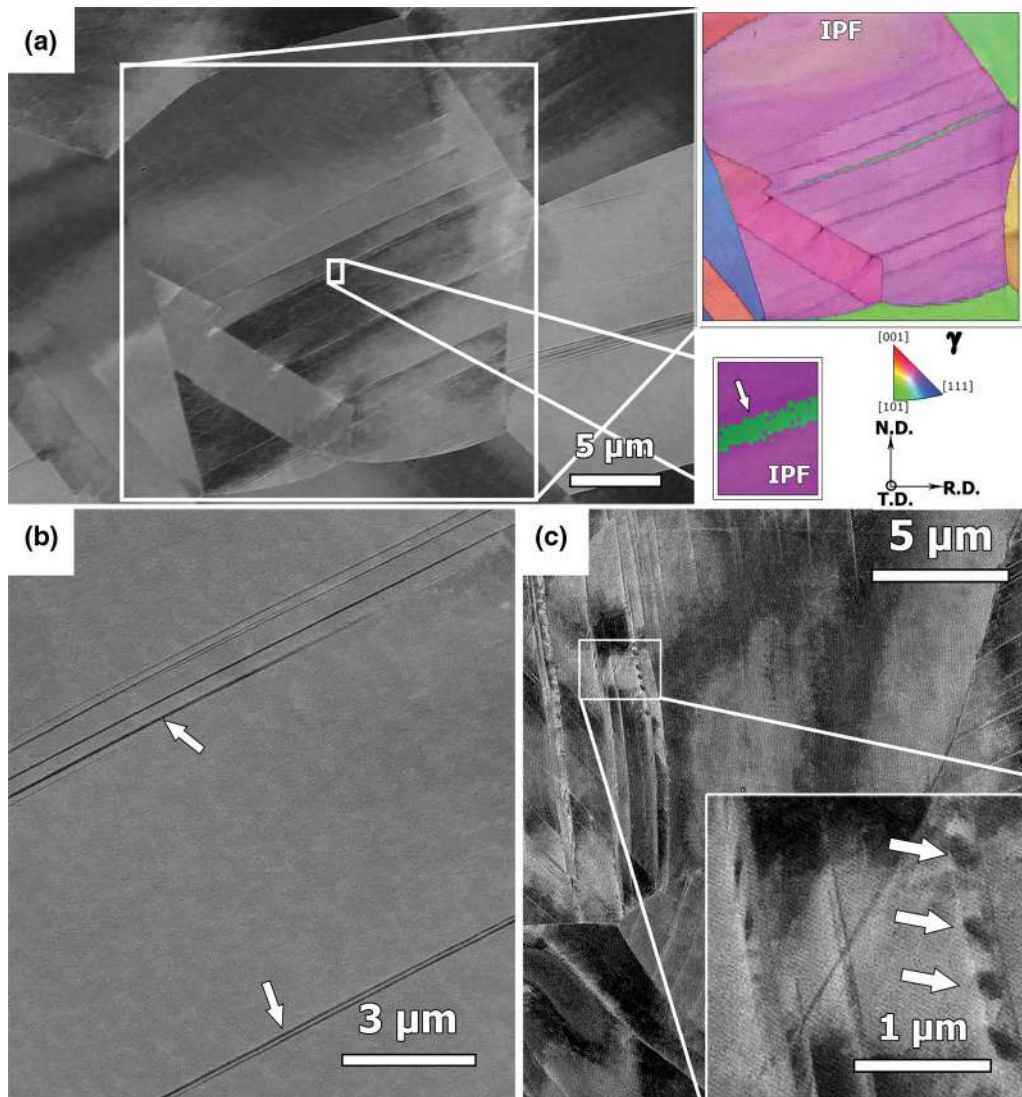
Fig. 3—IPF//N.D. and ECCI images of deformation structure at 10pct cold rolling reduction (*a* and *b*) and ECCI image of 20pct cold rolling reduction (*c*) for alloy 18-12.

formation from ε[29] which is the preferentially formed phase at low SFE during deformation.

Figure 3 shows the deformation structure of alloy 18-12 subjected to 10pct reduction. There are almost no α' or ε formed at this low degree of deformation. Instead, mechanical twinning is the dominant deformation mode (Figure 3a and b) (indicated by white arrows). It has been verified that twin intersections are preferred nucleation sites when mechanical twinning is the main deformation mechanism[16,20]; however, at low degree of deformation in the absence of ε, α' did not nucleate in the most stable alloy studied in this work. It should be noticed that for more severe deformation, when individual SBs are sometimes distorted or sheared, α' can form (white arrows in Figure 3(c)).

It has been demonstrated that ECCI combined with EBSD provides excellent insight into the deformation structure of Fe-Cr-Ni ternary alloys with the possibility to study large fields of view for good statistics. The ε is proved to play an important role in the deformation-induced α' martensitic transformation, especially making the nucleation at individual SBs possible. Without the help of ε, individual SBs consisting of only SFs and/or mechanical twins cannot facilitate α' formation; instead, intersection of SBs is required to lower the barrier for nucleation of α'.

The nucleation sites of α' and the deformation structure are related to the Ni composition and the SFE. Their relationship, at early stages of deformation, is summarized in Figure 4. For the rather unstable alloys with 10 wt pct Ni, and an estimated SFE of 6.6 mJ m^{-2}, blocky α' can form between adjacent sets of SBs, which indicates quite unstable austenite. Stacking faults, ε, and α' are found within these SBs, and for these alloys nucleation at individual SBs is frequently observed apart from that at intersections of SBs. For the more stable alloy with a higher nickel content between 11 and 11.5 wt pct (SFE estimated to be between 9.6 to 9.8 mJ m^{-2}), mechanical twins are more thermodynamically favorable during deformation and nucleation of α' at
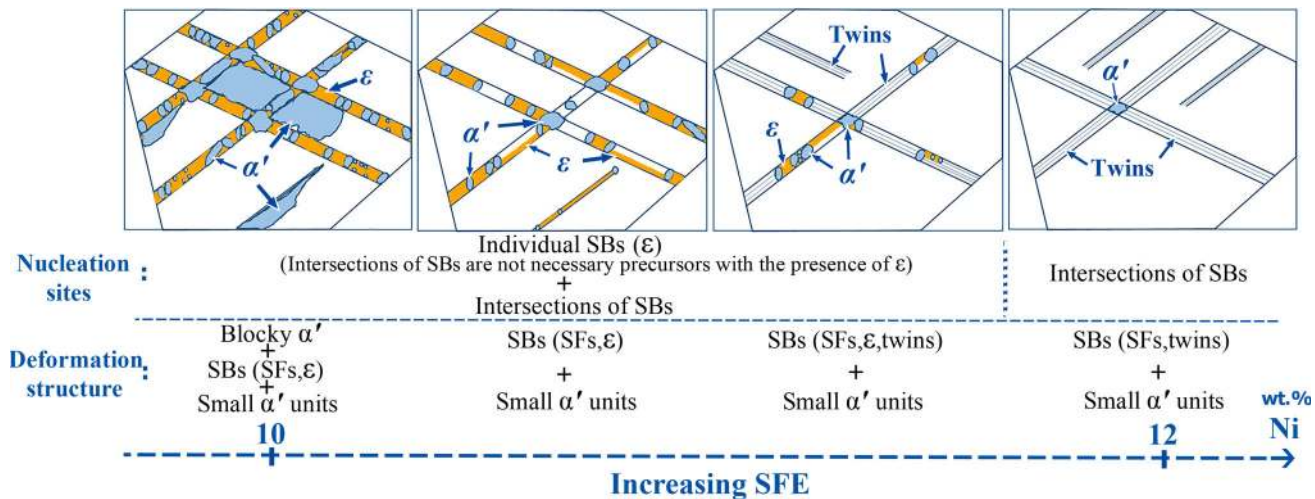
Fig. 4—Schematic diagram of the correlation between deformation structure and SFE in Fe-Cr-Ni alloys with Ni variation. SB: Shear band, SF: Stacking fault.

individual SBs is less frequent. This is due to the lower fraction of ε, since α' usually nucleates along ε where less activation energy is needed for its nucleation. For the alloy with the highest nickel content, *i.e.*, the 12 wt pct Ni (SFE estimated to be 12.4 mJ m^{-2}), only mechanical twins and SFs are found inside individual SBs with almost no α'. Further deformation may lead to the formation of some α' at the intersections of SBs and in some highly deformed areas.

REFERENCES

1. G.B. Olson and M. Cohen: *Metall. Trans. A*, 1975, vol. 6A, pp. 791–95.
2. D. Bhandarkar, V. Zackay, and E. Parker: *Metall. Mater. Trans. B*, 1972, vol. 3B, pp. 2619–31.
3. A. Das, S. Sivaprasad, M. Ghosh, P.C. Chakraborti, and S. Tarafder: *Mater. Sci. Eng. A*, 2008, vol. 486, pp. 283–86.
4. P. Hedström, L.E. Lindgren, J. Almer, U. Lienert, J. Bernier, M. Terner, and M. Odén: *Metall. Mater. Trans. A*, 2009, vol. 40A, pp. 1039–48.
5. L. Vitos, P. Korzhavyi, and B. Johansson: *Phys. Rev. Lett.*, 2006, vol. 96, p. 117210.
6. P. Ferreira and P. Müllner: *Acta Mater.*, 1998, vol. 46, pp. 4479–84.
7. G. Olson and M. Cohen: *J. Less Common Met.*, 1972, vol. 28, pp. 107–18.
8. K. Spencer, M. Véron, K. Yu-Zhang, and J.D. Embury: *Mater. Sci. Technol.*, 2009, vol. 25, pp. 7–17.
9. H. Schuman: *Krist. Technol.*, 1975, vol. 10, pp. 401–11.
10. M. Humbert, B. Petit, B. Bolle, and N. Gey: *Mater. Sci. Eng. A*, 2007, vols. 454–455, pp. 508–17.
11. T.-H. Lee, H.-Y. Ha, J.-Y. Kang, J. Moon, C.-H. Lee, and S.-J. Park: *Acta Mater.*, 2013, vol. 61, pp. 7399–7410.
12. J.F. Breedis and L. Kaufman: *Metall. Trans.*, 1971, vol. 2, pp. 2359–71.
13. P. Hedström, U. Lienert, J. Almer, and M. Odén: *Scr. Mater.*, 2007, vol. 56, pp. 213–16.
14. C.X. Huang, G. Yang, Y.L. Gao, S.D. Wu, and S.X. Li: *J. Mater. Res.*, 2007, vol. 22, pp. 724–29.
15. J. Talonen and H. Hänninen: *Acta Mater.*, 2007, vol. 55, pp. 6108–18.
16. L. Murr, K. Staudhammer, and S. Hecker: *Metall. Trans. A*, 1982, vol. 13, pp. 627–35.
17. J.-Y. Choi and W. Jin: *Scr. Mater.*, 1997, vol. 36, pp. 99–104.
18. F. Lecroisey and A. Pineau: *Metall. Trans.*, 1972, vol. 3, pp. 391–400.
19. H. Biermann, J. Solarek, and A. Weidner: *Steel Res. Int.*, 2012, vol. 83, pp. 512–20.
20. N. Nakada, H. Ito, Y. Matsuoka, T. Tsuchiyama, and S. Takaki: *Acta Mater.*, 2010, vol. 58, pp. 895–903.
21. D. Borisova, V. Klemm, S. Martin, S. Wolf, and D. Rafaja: *Adv. Eng. Mater.*, 2013, vol. 15, pp. 571–82.
22. N. Gey, B. Petit, and M. Humbert: *Metall. Mater. Trans. A*, 2005, vol. 36A, pp. 3291–99.
23. R. Naraghi, P. Hedström, and A. Borgenstam: *Steel Res. Int.*, 2011, vol. 82, pp. 337–45.
24. M. Chen, S. Gao, D. Terada, A. Shibata, and N. Tsuji: 2013, pp. 563–69.
25. E.S.S. Perdahcıoğlu, H.J.M.J.M. Geijselaers, and M. Groen: *Scr. Mater.*, 2008, vol. 58, pp. 947–50.
26. E.S. Perdahcioglu and H.J.M. Geijselaers: *Acta Mater.*, 2012, vol. 60, pp. 4409–19.

27. A. Das, P.C. Chakraborti, S. Tarafder, and H.K.D.H. Bhadeshia: *Mater. Sci. Technol.*, 2011, vol. 27, pp. 366–70.
28. A. Weidner, S. Martin, V. Klemm, U. Martin, and H. Biermann: *Scr. Mater.*, 2011, vol. 64, pp. 513–16.
29. S. Martin, S. Wolf, U. Martin, L. Krüger, and D. Rafaja: *Metall. Mater. Trans. A*, 2014, vol. 47A, pp. 49–58.
30. S. Zaefferer and N.-N. Elhami: *Acta Mater.*, 2014, vol. 75, pp. 20–50.
31. I. Gutierrez-Urrutia, S. Zaefferer, and D. Raabe: *Scr. Mater.*, 2009, vol. 61, pp. 737–40.
32. Y. Tian, A. Borgenstam, and P. Hedström: *Mater. Today Proc.*, 2015, vol. 2, pp. 687–90.
33. P.J.H. Denteneer and W. van Haeringen: *J. Phys. C Solid State Phys.*, 1987, vol. 20, p. L883.
34. L. Vitos: *Phys. Rev. B*, 2001, vol. 64, p. 14107.
35. L. Vitos, I.A. Abrikosov, and B. Johansson: *Phys. Rev. Lett.*, 2001, vol. 87, p. 156401.
36. A.V. Ruban, A.B. Belonoshko, and N.V. Skorodumova: *Phys. Rev. B*, 2013, vol. 87, pp. 1–6.
37. A. Reyes-Huamantinco, P. Puschnig, C. Ambrosch-Draxl, O.E. Peil, and A.V. Ruban: *Phys. Rev. B*, 2012, vol. 86, pp. 1–5.
38. J.P. Perdew, K. Burke, and M. Ernzerhof: *Phys. Rev. Lett.*, 1996, vol. 77, pp. 3865–68.
39. H.J. Monkhorst and J.D. Pack: *Phys. Rev. B*, 1976, vol. 13, pp. 5188–92.
40. I.A. Abrikosov, S.I. Simak, B. Johansson, A.V. Ruban, and H.L. Skriver: *Phys. Rev. B*, 1997, vol. 56, p. 9319.
41. O.E. Peil, A.V. Ruban, and B. Johansson: *Phys. Rev. B*, 2012, vol. 85, p. 165140.
42. A.V. Ruban and H.L. Skriver: *Phys. Rev. B*, 2002, vol. 66, p. 24201.
43. A.V. Ruban, S.I. Simak, P.A. Korzhavyi, and H.L. Skriver: *Phys. Rev. B*, 2002, vol. 66, p. 24202.
44. W. Li, S. Lu, D. Kim, K. Kokko, S. Hertzman, S.K. Kwon, and L. Vitos: *Appl. Phys. Lett.*, 2016, vol. 108, p. 081903.
45. A. Das: *Metall. Mater. Trans. A*, 2016, vol. 47A, pp. 748–68.
46. I.A. Abrikosov, A.V. Ponomareva, P. Steneteg, S.A. Barannikova, and B. Alling: *Curr. Opin. Solid State Mater. Sci.*, 2016, vol. 20, pp. 85–106.
47. F.D. Fischer, G. Reisner, E. Werner, K. Tanaka, G. Cailletaud, and T. Antretter: *Int. J. Plast.*, 2000, vol. 16, pp. 723–48.
48. K. Sato, M. Ichinose, Y. Hirotsu, and Y. Inoue: *ISIJ Int.*, 1989, vol. 29, pp. 868–77.
49. L. Remy and A. Pineau: *Mater. Sci. Eng.*, 1976, vol. 26, pp. 123–32.
50. S. Matsumoto, A. Sato, and T. Mori: *Acta Metall. Mater.*, 1994, vol. 42, pp. 1207–13.
51. T. Masumura, N. Nakada, T. Tsuchiyama, S. Takaki, T. Koyano, and K. Adachi: *Acta Mater.*, 2015, vol. 84, pp. 330–38.
52. A. Weidner, C. Segel, and H. Biermann: *Mater. Lett.*, 2015, vol. 143, pp. 155–58.